Computer Modeling in Engineering & Sciences

Tech Science Press

DOI: 10.32604/cmes.2023.029801

ARTICLE

Average Secrecy Capacity of the Reconfigurable Intelligent Surface-Assisted Integrated Satellite Unmanned Aerial Vehicle Relay Networks

Ping Li[1], Kefeng Guo[2,*], Feng Zhou[1], Xueling Wang[3] and Yuzhen Huang[4]

[1]School of Information Technology, Yancheng Institute of Technology, Yancheng, 224051, China

[2]School of Space Information, Space Engineering University, Beijing, 101407, China

[3]Space E-Star Communication Technology Co., Ltd, Nanjing, 210007, China

[4]Academy of Military Sciences of PLA, Beijing, 100097, China

*Corresponding Author: Kefeng Guo. Email: guokefeng.cool@163.com

Received: 09 March 2023 Accepted: 22 May 2023 Published: 17 November 2023

ABSTRACT

Integrated satellite unmanned aerial vehicle relay networks (ISUAVRNs) have become a prominent topic in recent years. This paper investigates the average secrecy capacity (ASC) for reconfigurable intelligent surface (RIS)-enabled ISUAVRNs. Especially, an eve is considered to intercept the legitimate information from the considered secrecy system. Besides, we get detailed expressions for the ASC of the regarded secrecy system with the aid of the reconfigurable intelligent. Furthermore, to gain insightful results of the major parameters on the ASC in high signal-to-noise ratio regime, the approximate investigations are further gotten, which give an efficient method to value the secrecy analysis. At last, some representative computer results are obtained to prove the theoretical findings.

KEYWORDS

Integrated satellite unmanned aerial vehicle relay networks; reconfigurable intelligent surface; average secrecy capacity (ASC); asymptotic ASC

1 Introduction

The future requirements of wireless communication networks have so many characters, such as wider coverage, higher energy utilization, et al. Wider coverage has become an important requirement for the wireless networks [1]. Based on this consideration, satellite communication (SatCom) comes to our insight for its ubiquitous coverage and seamless services for several users [2]. Thus, by both using the superiorities of the SatCom and terrestrial communication networks (TCNs), integrated satellite terrestrial networks (ISTNs) arise, which can not only use the advantage of the SatCom but also utilize TCNs. They are considered as the future structure of the next generation wireless communication system [3–5]. ISTNs have been considered as the important part in the practical systems, such as Digital Video Broadcasting (DVB) networks and the Space-Ground Integrated Information Network Engineering of China [6–9].

1.1 Related Works

As mentioned previously, the ISTN has been regarded as a hot research topic these years. In [10], the authors researched the outage probability (OP) for a representative ISTN along with several terrestrial relays by applying the threshold-assisted selection algorithm. The authors in [11] researched the OP for a representative uplink ISTN with the opportunistic terrestrial selection algorithm. In [12], the authors studied the OP for ISTNs with the proposed maximal-maximum terrestrial selection scheme. The authors in [13] studied the symbol error rate for an ISTN. As known, the SatCom has a wider coverage, which results into the appearance of the secrecy problem. By utilizing the different method, physical layer security (PLS) mainly researches the divergence between the legitimate user's channel and the eavesdropper's channel [14,15]. The authors in [15] summarized all the secrecy problems in the SatCom and gave some promising secrecy researching directions. In [16], the authors researched the security problem for a cognitive ISTN by applying beamforming (BF) scheme. The authors in [17] proposed a threshold-based legitimate users scheduling algorithm for an ISTN with several legitimate users and several eavesdroppers. In [18], the authors obtained the detailed investigations for the secrecy outage probability (SOP) of the ISTNs along with a two-way unmanned-aerial-vehicle (UAV). In [19], the authors studied the SOP for an ISTN with non-orthogonal multiple access (NOMA) technique by also considering the cognitive technology. In [20], a cooperative relay selection and legitimate user selection algorithm was proposed and the average secrecy capacity (ASC) was investigated in a considered ISTN. The authors in [21] proposed a BF algorithm to optimize the secrecy performance of an ISTN. In [22], the authors proposed an alternating optimization scheme to address the SEE problem by decomposing the original nonconvex problem into subproblems.

1.2 Motivations

Another important demand for the 6G network and next wireless communication network is higher energy efficiency, which has been an important factor for the urban networks [23]. On this foundation, reconfigurable intelligent surface (RIS) technology comes to our sight. The RIS is the man-made surface which can reflect the signal by setting the suitable phase with the special electronic material [24]. It will need nearly no power to reflect the legitimate signal, which is now the famous topic in recent five years [25,26]. The authors in [27] researched the OP of the UAV-assisted communication networks. In [28], the authors minimized the transmission power for the representative UAV-based RIS-assisted hetnets. The authors in [29] studied the effect of RIS and UAV relay on the ISTNs. In [30], the authors researched the impacts of hardware impairments and RIS on the considered ISTNs in the presence of a UAV relay. Besides, the insightful investigation for the OP was studied. In [31], the authors investigated the joint beamforming problems for a representative ISTN. In [32], the authors studied the impact of NOMA scheme on a representative ISTN in the presence of cognitive technology.

By summarizing all and trying the authors' best efforts, the study for the effect of RIS-based ISTN with a UAV on the ASC remains unreported, which motivates our work.

1.3 Our Contributions

Accordingly, this paper first considers the UAV relay and an eavesdropper. Specifically, the RIS is mounted on a tall building to augment the transmission. Then, we research the ASC for the considered network. The detailed works of this paper are given in what follows as

- By taking the satellite, the UAV, the legitimate user and an eavesdropper into consideration, the considered secrecy network appears. Furthermore, in order to enhance the secrecy transmission and improve the energy utilization, the RIS is stalled in the high building to help the UAV. In addition, the decode-and-forward (DF) forwarding method is used at the UAV to assist the

satellite' transmission. For some practical reasons, the direct transmission link does not exist in the considered network, namely, the satellite can not communicate with the legitimate user directly.

- Relied on the considered networks, detailed investigations for the ASC are obtained. The detailed investigations provide efficient methods to evaluate the effects of key parameters, i.e., the channel and system parameters on the ASC. Especially, these derivations can derive the impacts of RIS' parameters.
- To gain further investigations of the ASC on the considered networks, the asymptotic investigations for the ASC are gotten, which give deep insights on the considered secrecy networks.

The structure of this paper is as follows. Through Section 2, the detailed illustration of regarded secrecy system model is provided. In Section 3, the deep investigations for the ASC are provided along with the closed-form expressions. In Section 4, the asymptotic analysis is further obtained. In Section 5, some representative Monte Carlo simulations are given to see the rightness of the analytical investigations. The summary of this work is given in Section 6.

Notations $|\cdot|$ depicts the absolute value of a complex scalar. $E[\cdot]$ represents the expectation function, $\mathscr{CN}(\mathbf{a}, \mathbf{B})$ depicts the complex Gaussian distribution, which consists of a random vector $\mathbf{a}$ and covariance matrix $\mathbf{B}$. $F_y(\cdot)$ and $f_y(\cdot)$ represent the cumulative distribution function (CDF) and probability density function (PDF) the of random variable y, respectively. The abbreviations are given in Table 1.

Table 1: Abbreviations

SatCom	Satellite communication
TCNs	Terrestrial communication networks
UAV	Unmanned-aerial-vehicle
OP	Outage probability
PLS	Physical layer security
ISTNs	Integrated satellite terrestrial networks
AWGN	Additive white Gaussian noise
BF	Beamforming
SOP	Secrecy outage probability
NOMA	Non-orthogonal multiple access
ASC	Average secrecy capacity
RIS	Reconfigurable intelligent surface
DF	Decode-and-froward
SR	Shadowed-Rician
PDF	Probability density function
LoS	Line of sight
SNR	Signal-to-noise ratio
FSL	Free space loss
LMS	Land mobile satellite
CDF	Cumulative distribution function
MC	Monte Carlo
FHS	Frequency heavy shadowing

(Continued)

Table 1 (continued)

SatCom	Satellite communication
AS	Average shadowing
TDMA	Time division multiple access
GEO	Geosynchronous earth orbit
ILS	Infrequent light shadowing
i.i.d	Independent and identically distribution
LMS	Land mobile satellite

2 System Model

As shown in Fig. 1, through this secrecy RIS-assisted ISTN, it includes a satellite S, a legitimate user D and a DF UAV[1] relay R. Besides, a RIS is equipped in a high structure to forward the signal. In this considered network, one antenna is considered for the whole network nodes[2]. As the former presentation, the satellite and UAV both own a wider beam coverage, thus an eavesdropper exists in the considered model and wants to steal the information signal from the UAV. Owing to the shadowing and so many problems, not any direct transmitting link is available in this paper, namely, D cannot receive the information from S and cannot receive the signal from R directly[3].

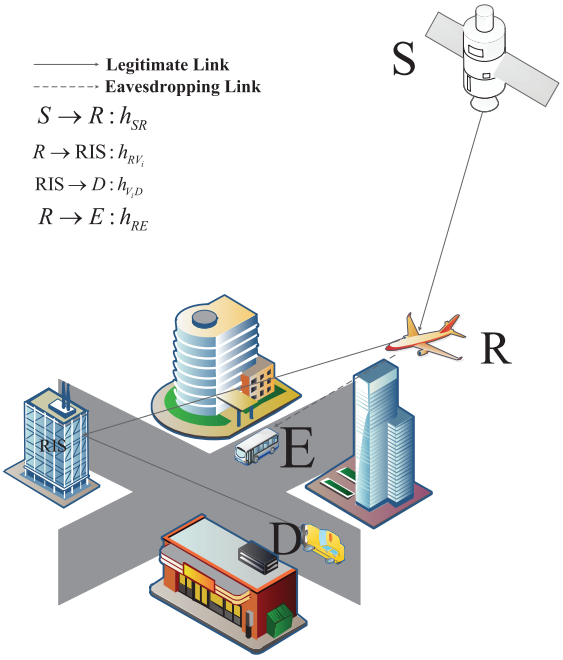

Figure 1: The system model illustration

[1] Although in this paper, we just use only one UAV, the obtained results can also suit for the case with multiple UAVs.
[2] It is mentioned that, in this paper, each node owns only one antenna, while the remaining results are also suitable to the case that transmission nodes having multiple antennas when beamforming (BF) is utilized at the multiple antenna node.
[3] Owing to obstacles, fogs, rain attenuation, in this paper direct transmission link between the source and destination is not available, which will be considered in our future works.

Two time slots will last for the whole link. In the first one, S forwards the symbol $s(t)$ with $E\left[|s(t)|^2\right]=1$ to R, thus the obtained signal at R can be regarded as

$$y_{SR}(t)=\sqrt{P_S}h_{SR}s(t)+n_R(t), \tag{1}$$

where P_S depicts the transmitting energy of S, h_{SR} represents the channel fading between the S and R which suffers from shadowed-Rician (SR), $n(t)$ depicts the additive white Gaussian noise (AWGN) at R which has the model as $n_R(t)\sim\mathscr{CN}\left(0,\delta_R^2\right)$.

For the second one, R intends to transmit the legitimate information signal to D. Unfortunately, due to some reasons, such as obstacles, R cannot transmit the singal with D directly. So, RIS is utilized to assist the legitimate transmitting. Then, the final signal at D is represented with the expression as

$$y_{RD}(t)=\sqrt{P_R}\left[\sum_{i=1}^{N}h_{RX_i}e^{j\theta_i}h_{X_iD}\right]s(t)+n_D(t), \tag{2}$$

where P_R depicts the transmitting power from R, N is the number of the reflecting factor, θ_i depicts the phase shift of the i-th factor for the RIS. h_{RX_i} and h_{X_iD} represent the channel function with presentation as $h_{RX_i}=\beta_i e^{-\phi_i}/\sqrt{L_{RX_i}}$ and $h_{X_iD}=\tau_i e^{-\psi_i}/\sqrt{L_{X_iD}}$, respectively. β_i and τ_i denote the random variable which undergoes Rayleigh fading with a $\sqrt{\pi}/2$ mean and a $(4-\pi)/4$ variance. $L_{RX_i}=10\log 10\left(l_{RX_i}^{\varphi}\right)+B$ and $L_{X_iD}=10\log 10\left(l_{X_iD}^{\varphi}\right)+B$ represent the path loss, B denotes the a target value which has a relationship with the transmitting frequency and some other issues. l_{X_iD} and l_{RX_i} denote the distance of the RIS-D and R-RIS links, respectively, φ represents the path loss value. $n_D(t)$ denotes the AWGN at D shadowed as $n_D(t)\sim\mathscr{CN}\left(0,\delta_D^2\right)$ [30].

By utilizing [33], the best performance signal for the RIS $\rightarrow$ D link can be obtained by setting $\theta_i=\phi_i+\psi_i$, which can be shown as

$$y_{RD}(t)=\sqrt{P_R}\left(\underbrace{\sum_{i=1}^{N}\beta_i\tau_i/\sqrt{L_{RX_i}L_{X_iD}}}_{\chi}\right)s(t)+n_D(t). \tag{3}$$

As mentioned before, a secrecy problem exists in the considered networks. Thus, the information overheard by the Eve is shown as

$$y_{RE}(t)=\sqrt{P_R}h_{RE}s(t)+n_E(t), \tag{4}$$

where h_{RE} represents the channel shadowing between R and E with modeling as Rayleigh fading, $n_E(t)$ represents the AWGN at E obeyed as $n_E(t)\sim\mathscr{CN}\left(0,\delta_E^2\right)$.

From (1), (3) and (4), the obtained signal-to-noise ratios (SNRs) for the different links are respectively given by

$$\gamma_{SR}=\frac{P_S|h_{SR}|^2}{\delta_R^2}, \tag{5}$$

$$\gamma_{RD}=\frac{P_R\chi^2}{L_{RX_i}L_{X_iD}\delta_D^2}, \tag{6}$$

$$\gamma_E = \frac{P_R |h_{RE}|^2}{\delta_E^2}. \tag{7}$$

For the reason that DF protocol is applied for the UAV, then the legitimate SNR of the secrecy system is obtained as

$$\gamma_B = \min(\gamma_{SR}, \gamma_{RD}). \tag{8}$$

Relied on [14], the secrecy capacity has the following definition as

$$C_S = \lfloor C_B - C_E \rfloor^+, \tag{9}$$

where $\lfloor x \rfloor^+ \triangleq \max\{x, 0\}$, $C_B = \log_2(1 + \gamma_B)$ and $C_E = \log_2(1 + \gamma_E)$.

3 Average Secrecy Capacity

From [17], the ASC is regarded as

$$\begin{aligned} \overline{C}_S &= \int_0^\infty \int_0^\infty C_S f_{\gamma_B}(x) f_{\gamma_E}(z)\, dxdz \\ &= \int_0^\infty \int_0^\infty [\log_2(1+x) - \log_2(1+z)] f_{\gamma_B}(x) f_{\gamma_E}(z)\, dxdz \\ &= \frac{1}{\ln 2} \int_0^\infty \frac{F_{\gamma_E}(z)}{1+z} \left[1 - F_{\gamma_B}(z)\right] dz. \end{aligned} \tag{10}$$

Before getting the final derivations of ASC, the first important one is to gain the CDF and PDF for γ_{SR}, γ_{RD} and γ_E, respectively.

3.1 Preliminaries

3.1.1 The Satellite Transmission Model

Through this paper, the geosynchronous earth orbit (GEO)[4] satellite is assumed. In addition, the satellite is considered to own many transmission beams. Moreover, time division multiple access (TDMA)[5] algorithm is inserted which leads to result that just one UAV is used in each time slot.

Then, h_{SR} is expressed as

$$h_{SR} = C_{SR} f_{SR}, \tag{11}$$

where f_{SR} depicts the SR fading of the satellite shaodwing, and C_{SR} depicts the impact of antenna pattern and the free space loss (FSL), which can be represented as

$$C_{SR} = \frac{\lambda \sqrt{G_{SR} G_R}}{4\pi \sqrt{d^2 + d_0^2}}, \tag{12}$$

[4]Although in this paper, we take the GEO satellite for an example, the obtained investigations can be also used to the scenario with medium Earth orbit (MEO) and low Earth orbit (LEO) satellites.

[5]TDMA scheme is used in the satellite to keep only one satellite beam and one UAV is used in each data transmission time slot. TDMA scheme is both adopted for the satellite downlink and uplink data transmission.

where λ represents the frequency carrier's wavelength, d is the length from terrestrial relay to the satellite beam's center with $d = d_0 \tan(\overline{\theta}_k)$. $\bar{\theta}_k$ is regarded as the 3 dB angle. $d_0 \approx 35786$ km is the antenna gain for terrestrial relay. Furthermore, G_R depicts the beam gain of the considered satellite.

From [17], G_R can be approximated as

$$G_R(dB) \simeq \begin{cases} \overline{G}_{\max}, & for\ 0^\circ < \vartheta < 1^\circ \\ 32 - 25\log\vartheta, & for\ 1^\circ < \vartheta < 48^\circ \\ -10, & for\ 48^\circ < \vartheta \leq 180^\circ, \end{cases} \tag{13}$$

where $\overline{G}_{\max}$ represents the maximum beam gain, and ϑ denotes the off-boresight's angle. Considering G_{SR} as the gain of the antenna, by assuming θ_k being the angle, which is shown as [2,19]

$$G_{SR} \simeq G_{\max}\left(\frac{K_1(u_k)}{2u_k} + 36\frac{K_3(u_k)}{u_k^3}\right), \tag{14}$$

where G_{max} depicts the best beam gain, $u_k = 2.07123 \sin\theta_k / \sin\overline{\theta}_k$, K_3 and K_1 are the order 3 and 1 for the 1st-kind bessel function, respectively. To derive the best performance, $\theta_k \to 0$ is applied which leads to $G_{SR} \approx G_{\max}$. After which consideration, we get $h_{SR} = C_{SR}^{\max} f_{SR}$.

For f_{SR}, a popular SR model was mentioned in [34] that suits for land mobile satellite (LMS) networks [17]. By using [2], f_V could be re-given as $f_{SR} = \overline{f}_{SR} + \widetilde{f}_{SR}$, where $\widetilde{f}_{SR}$ has the assumption as independent identically distributed (i.i.d) Rayleigh shadowing, $\overline{f}_{SR}$ represents the effect of line-of-sight (LoS) issue which undergoes i.i.d Nakagami-m fading.

By utilizing [34], the PDF and CDF of $\gamma_{SR} = \overline{\gamma}_S R \left| C_{SR}^{\max} f_{SR} \right|$ are respectively obtained as

$$f_{\gamma_{SR}}(x) = \sum_{k_1=0}^{m_{SR}-1} \frac{\alpha_{SR}(1-m_{SR})_{k_1}(-\delta_{SR})^{k_1} x^{k_1}}{(k_1!)^2 \bar{\gamma}_{SR}^{k_1+1} \exp(\Delta_{SR} x)}, \tag{15}$$

$$F_{\gamma_{SR}}(x) = 1 - \sum_{k_1=0}^{m_{SR}-1} \sum_{t=0}^{k_1} \frac{\alpha_{SR}(1-m_{SR})_{k_1}(-\delta_{SR})^{k_1} x^t}{k_1!\, t!\, \bar{\gamma}_{SR}^{k_1+1} \Delta_{SR}^{k_1-t+1} \exp(\Delta_{SR} x)}. \tag{16}$$

where $\overline{\gamma}_{SR}$ depicts the average SNR between S and R, $\Delta_{SR} = \dfrac{\beta_{SR} - \delta_{SR}}{\overline{\gamma}_{SR}}$, $\alpha_{SR} = \left(\dfrac{2b_{SR}m_{SR}}{2b_{SR}m_{SR} + \Omega_{SR}}\right)^{m_{SR}} / 2b_{SR}$, $\beta_{SR} = 1/2b_{SR}$, $\delta_{SR} = \dfrac{\Omega_{SR}}{(2b_{SR}m_{SR} + \Omega_{SR})\, 2b_{SR}}$, where $m_{SR} \geq 0$ denotes the fading factor, $2b_{SR}$ represents the multipath's power. In addition, Ω_{SR} denotes the LoS link's power. As a common consideration, m_{SR} is assumed to be an integer [18]. $(\cdot)_{k_1}$ represents the Pochhammer symbol [35].

3.1.2 The RIS Channel Model

Then, by utilizing [30], the PDF and CDF for γ_{RD} are respectively presented as

$$f_{\gamma_{RD}}(x) \simeq \frac{e^{-\frac{\left(x - \overline{\gamma}_{RD^s}\right)^2}{2\delta^2 \overline{\gamma}_{RD}^2}}}{\sqrt{2\pi\delta^2 \overline{\gamma}_{RD}^2}}, \tag{17}$$

$$F_{\gamma_{RD}}(x) = \frac{1}{\sqrt{2\pi\delta^2\overline{\gamma}_{RD}^2}}\left[\Phi(A,B,C,x) - \Phi(A,B,C,0)\right], \tag{18}$$

where

$$\Phi(A,B,C,x) = \frac{1}{2}\sqrt{\pi/A}\exp\left(\frac{B^2-AC}{A}\right) erf\left(\sqrt{A}x + B/\sqrt{A}\right), \tag{19}$$

and $s = N\pi/4$ and $\delta^2 = N\left(1-\pi^2/16\right)$, $A = \dfrac{1}{2\delta^2\overline{\gamma}_{RD}^2}$, $B = \dfrac{-s}{2\delta^2\overline{\gamma}_{RD}}$ and $C = \dfrac{s^2}{2\delta^2}$, and $erf(x)$ denotes the error function shown in [35]. $\bar{\gamma}_{RD}$ depicts the average SNR from R to D.

From [35], $erf(x)$ can be obtained as

$$erf(x) = \frac{2}{\sqrt{\pi}}\sum_{k=1}^{\infty}\frac{x^{2k-1}(-1)^{k+1}}{(k-1)!(2k-1)}. \tag{20}$$

3.1.3 The Terrestrial Channel Model

By utilizing the similar method, from [10], the PDF for γ_E has the expression as

$$F_{\gamma_E}(x) = 1 - \exp\left(-x/\overline{\gamma}_E\right). \tag{21}$$

3.2 The ASC

Recalling (10), the first thing that needs to be done is to get the CDF of γ_E and the CDF of γ_B. The CDF of γ_E has been derived in (21), by utilizing the DF protocol and [33], the CDF for γ_B can be derived as

$$F_{\gamma_B}(x) = 1 - \Theta_1 - H\Theta_1 + \Theta_2, \tag{22}$$

with

$$H = \frac{1}{\sqrt{2\pi A\delta^2\bar{\gamma}_{RD}^2}}\exp\left(\frac{B^2-AC}{A}\right)\sum_{k=1}^{\infty}\frac{(-1)^{k+1}B^{2k-1}}{A^{k-1/2}(k-1)!(2k-1)}, \tag{23}$$

$$\Theta_1 = \sum_{k_1=0}^{m_{SR}-1}\sum_{t=0}^{k_1}\frac{\alpha_{SR}(1-m_{SR})_{k_1}(-\delta_{SR})^{k_1}x^t}{k_1!\,t!\,\bar{\gamma}_{SR}^{k_1+1}\Delta_{SR}^{k_1-t+1}\exp(\Delta_{SR}x)}, \tag{24}$$

and

$$\Theta_2 = \sum_{k_1=0}^{m_{SR}-1}\sum_{t=0}^{k_1}\sum_{k=1}^{\infty}\sum_{p}^{2k-1}\frac{\binom{2k-1}{p}B^{2k-1-p}(-1)^{k+1}x^{t+p}\alpha_{SR}(1-m_{SR})_{k_1}(-\delta_{SR})^{k_1}\exp\left(\frac{B^2-AC}{A}\right)}{A^{k-1/2-p}(k-1)!(2k-1)\sqrt{2\pi a\delta^2\bar{\gamma}_{RD}^2}k_1!\,t!\,\bar{\gamma}_{SR}^{k_1+1}\Delta_{SR}^{k_1-t+1}\exp(\Delta_{SR}x)}. \tag{25}$$

By submitting (22) and (21) into (10), (10) can be re-written as

$$
\begin{aligned}
C_S &= \frac{1}{\ln 2}\int_0^{\infty}\frac{1-\exp\left(-z/\overline{\gamma}_E\right)}{1+z}\left(\Theta_1+H\Theta_1-\Theta_2\right)dz \\
&= \frac{1}{\ln 2}\int_0^{\infty}\frac{(1+H)\,\Theta_1-\Theta_2}{1+z}dz-\frac{1}{\ln 2}\int_0^{\infty}\frac{\exp\left(-z/\overline{\gamma}_E\right)(1+H)\,\Theta_1-\exp\left(-z/\overline{\gamma}_E\right)\Theta_2}{1+z}dz \\
&= \frac{1}{\ln 2}\int_0^{\infty}\frac{(1+H)\,\Theta_1}{1+z}dz-\frac{1}{\ln 2}\int_0^{\infty}\frac{\Theta_2}{1+z}dz-\frac{1}{\ln 2}\int_0^{\infty}\frac{\exp\left(-z/\overline{\gamma}_E\right)(1+H)\,\Theta_1}{1+z}dz \\
&\quad+\frac{1}{\ln 2}\int_0^{\infty}\frac{\exp\left(-z/\overline{\gamma}_E\right)\Theta_2}{1+z}dz \\
&= J_1-J_2-J_3+J_4,
\end{aligned}
\tag{26}
$$

where

$$
J_1=\frac{1+H}{\ln 2}\int_0^{\infty}\frac{\Theta_1}{1+z}dz=\sum_{k_1=0}^{m_{SR}-1}\sum_{t=0}^{k_1}\frac{\alpha_{SR}(1-m_{SR})_{k_1}(-\delta_{SR})^{k_1}\,(1+H)}{\ln 2k_1!\,t!\,\bar{\gamma}_{SR}^{k_1+1}\Delta_{SR}^{k_1-t+1}}\,Y\left(t,\Delta_{SR},1\right),
$$

$$
\begin{aligned}
J_2 &= \frac{1}{\ln 2}\int_0^{\infty}\frac{\Theta_2}{1+z}dz \\
&= \sum_{k_1=0}^{m_{SR}-1}\sum_{t=0}^{k_1}\sum_{k=1}^{\infty}\sum_{p}^{2k-1}\frac{\binom{2k-1}{p}B^{2k-1-p}(-1)^{k+1}\alpha_{SR}(1-m_{SR})_{k_1}(-\delta_{SR})^{k_1}\,Y\left(t+p,\Delta_{SR},1\right)}{\ln 2A^{k-1/2-p}\,(k-1)\,!\,(2k-1)\,\sqrt{2\pi a\delta^2\bar{\gamma}_{RD}^2}k_1!\,t!\,\bar{\gamma}_{SR}^{k_1+1}\Delta_{SR}^{k_1-t+1}\exp\left(\frac{AC-B^2}{A}\right)},
\end{aligned}
$$

$$
J_3=\frac{1+H}{\ln 2}\int_0^{\infty}\frac{\Theta_1 e^{\left(-\frac{z}{\bar{\gamma}_E}\right)}}{1+z}dz=\sum_{k_1=0}^{m_{SR}-1}\sum_{t=0}^{k_1}\frac{\alpha_{SR}(1-m_{SR})_{k_1}e^{\left(\frac{z}{\bar{\gamma}_E}\right)}\,(1+H)}{\ln 2k_1!\,t!\,\bar{\gamma}_{SR}^{k_1+1}\Delta_{SR}^{k_1-t+1}(-\delta_{SR})^{-k_1}}\,Y\left(t,\Delta_{SR}+1/\bar{\gamma}_E,1\right),
$$

$$
\begin{aligned}
J_4 &= \frac{1}{\ln 2}\int_0^{\infty}\frac{\Theta_2 e^{\left(-\frac{z}{\bar{\gamma}_E}\right)}}{1+z}dz \\
&= \sum_{k_1=0}^{m_{SR}-1}\sum_{t=0}^{k_1}\sum_{k=1}^{\infty}\sum_{p}^{2k-1}\frac{\binom{2k-1}{p}B^{2k-1-p}(-1)^{k+1}\alpha_{SR}(1-m_{SR})_{k_1}(-\delta_{SR})^{k_1}\exp\left(\frac{B^2-AC}{A}\right)}{\ln 2A^{k-1/2-p}\,(k-1)\,!\,(2k-1)\,\sqrt{2\pi a\delta^2\bar{\gamma}_{RD}^2}k_1!\,t!\,\bar{\gamma}_{SR}^{k_1+1}\Delta_{SR}^{k_1-t+1}e^{\left(-\frac{z}{\bar{\gamma}_E}\right)}} \\
&\quad\times Y\left(t+p,\Delta_{SR}+1/\bar{\gamma}_E,1\right),
\end{aligned}
\tag{27}
$$

where

$$
Y\left(n,u,b\right)=(-1)^{n-1}b^n e^{bu}Ei\left(-bu\right)+\sum_{p=1}^{n}\left(p-1\right)!\,(-b)^{n-p}u^{-p}.
\tag{28}
$$

Then, the detailed expression for the ASC of the regarded secrecy system is given by

$$\begin{aligned}\overline{C}_S = &\sum_{k_1=0}^{m_{SR}-1}\sum_{t=0}^{k_1}\frac{\alpha_{SR}(1-m_{SR})_{k_1}(-\delta_{SR})^{k_1}(1+H)}{\ln 2 k_1!\, t!\, \bar{\gamma}_{SR}^{k_1+1}\Delta_{SR}^{k_1-t+1}} Y(t,\Delta_{SR},1)\\ &-\sum_{k_1=0}^{m_{SR}-1}\sum_{t=0}^{k_1}\frac{\alpha_{SR}(1-m_{SR})_{k_1}e^{\left(\frac{z}{\bar{\gamma}_E}\right)}(1+H)}{\ln 2 k_1!\, t!\, \bar{\gamma}_{SR}^{k_1+1}\Delta_{SR}^{k_1-t+1}(-\delta_{SR})^{-k_1}} Y(t,\Delta_{SR}+1/\bar{\gamma}_E,1)\\ &-\sum_{k_1=0}^{m_{SR}-1}\sum_{t=0}^{k_1}\sum_{k=1}^{\infty}\sum_{p}^{2k-1}\frac{\binom{2k-1}{p}B^{2k-1-p}(-1)^{k+1}\alpha_{SR}(1-m_{SR})_{k_1}(-\delta_{SR})^{k_1}Y(t+p,\Delta_{SR},1)}{\ln 2 A^{k-1/2-p}(k-1)!\,(2k-1)\sqrt{2\pi a\delta^2\bar{\gamma}_{RD}^2}k_1!\, t!\, \bar{\gamma}_{SR}^{k_1+1}\Delta_{SR}^{k_1-t+1}\exp\left(\frac{AC-B^2}{A}\right)}\\ &+\sum_{k_1=0}^{m_{SR}-1}\sum_{t=0}^{k_1}\sum_{k=1}^{\infty}\sum_{p}^{2k-1}\frac{\binom{2k-1}{p}B^{2k-1-p}(-1)^{k+1}\alpha_{SR}(1-m_{SR})_{k_1}(-\delta_{SR})^{k_1}\exp\left(\frac{B^2-AC}{A}\right)}{\ln 2 A^{k-1/2-p}(k-1)!\,(2k-1)\sqrt{2\pi a\delta^2\bar{\gamma}_{RD}^2}k_1!\, t!\, \bar{\gamma}_{SR}^{k_1+1}\Delta_{SR}^{k_1-t+1}e^{\left(-\frac{z}{\bar{\gamma}_E}\right)}}\\ &\times Y(t+p,\Delta_{SR}+1/\bar{\gamma}_E,1). \end{aligned} \tag{29}$$

3.3 *Asymptotic ASC*

In the following, the asymptotic analysis for the ASC will be given. When SNR becomes lager enough, namely, $\bar{\gamma}_{SR}$ and $\bar{\gamma}_{RD}$ become infinite, the CDF of γ_{SR} and γ_{RD} are respectively derived as

$$F_{SR}(x) = \frac{\alpha_{SR}}{\overline{\gamma}_{SR}}x + o(x), \tag{30}$$

$$F_{\gamma_{RD}}(x) = e^{-\frac{s^2}{2\sigma^2}}x/\sqrt{2\pi\sigma^2\bar{\gamma}_{RD}^2} + o(x), \tag{31}$$

where $o(x)$ represents the higher order of x.

Thus, by utilizing (8), (30) and (31), the CDF of γ_B will be given as

$$F_{\gamma_B}(x) \simeq \frac{\alpha_{SR}}{\overline{\gamma}_{SR}}x + \frac{e^{-\frac{s^2}{2\sigma^2}}x}{\sqrt{2\pi\sigma^2\bar{\lambda}_{RD}^2}} + o(x). \tag{32}$$

By replacing (22) with (32), then submitting (32) and (21) into (10), the asymptotic investigations for ASC can be derived. Unfortunately, we find it that we can not get the final expression by utilizing this method. So, referring to (28), from the fact that when $\bar{\gamma}$ becomes larger enough, $\exp\left(\frac{x}{\bar{\gamma}}\right) \approx 1+\frac{x}{\bar{\gamma}}$ and $\frac{A}{\overline{\gamma}} + B \approx B$, namely, when $u \to 0$, (28) can be approximated as

$$Y^{\infty}(n,u,b) = \underbrace{Y(n,u,b)}_{u\to 0} = (-1)^{n-1}b^n(1+bu)\,Ei(-bu) + \sum_{p=1}^{n}(p-1)!\,(-b)^{n-p}u^{-p}. \tag{33}$$

Then, by utilizing (29) and (33), the asymptotic expression will be given by

$$\overline{C}_S^{\infty} = \sum_{k_1=0}^{m_{SR}-1}\sum_{t=0}^{k_1}\frac{\alpha_{SR}(1-m_{SR})_{k_1}(-\delta_{SR})^{k_1}(1+H)}{\ln 2 k_1!\, t!\, \bar{\gamma}_{SR}^{k_1+1}\Delta_{SR}^{k_1-t+1}} Y^{\infty}(t,\Delta_{SR},1)$$
$$-\sum_{k_1=0}^{m_{SR}-1}\sum_{t=0}^{k_1}\frac{\alpha_{SR}(1-m_{SR})_{k_1}e^{\left(\frac{z}{\bar{\gamma}_E}\right)}(1+H)}{\ln 2 k_1!\, t!\, \bar{\gamma}_{SR}^{k_1+1}\Delta_{SR}^{k_1-t+1}(-\delta_{SR})^{-k_1}} Y(t,1/\bar{\gamma}_E,1)$$
$$-\sum_{k_1=0}^{m_{SR}-1}\sum_{t=0}^{k_1}\sum_{k=1}^{\infty}\sum_{p}^{2k-1}\frac{\binom{2k-1}{p}B^{2k-1-p}(-1)^{k+1}\alpha_{SR}(1-m_{SR})_{k_1}(-\delta_{SR})^{k_1}Y^{\infty}(t+p,\Delta_{SR},1)}{\ln 2 A^{k-1/2-p}(k-1)!(2k-1)\sqrt{2\pi a\delta^2\bar{\gamma}_{RD}^2}k_1!\, t!\, \bar{\gamma}_{SR}^{k_1+1}\Delta_{SR}^{k_1-t+1}\exp\left(\frac{AC-B^2}{A}\right)}$$
$$+\sum_{k_1=0}^{m_{SR}-1}\sum_{t=0}^{k_1}\sum_{k=1}^{\infty}\sum_{p}^{2k-1}\frac{\binom{2k-1}{p}B^{2k-1-p}(-1)^{k+1}\alpha_{SR}(1-m_{SR})_{k_1}(-\delta_{SR})^{k_1}\exp\left(\frac{B^2-AC}{A}\right)}{\ln 2 A^{k-1/2-p}(k-1)!(2k-1)\sqrt{2\pi a\delta^2\bar{\gamma}_{RD}^2}k_1!\, t!\, \bar{\gamma}_{SR}^{k_1+1}\Delta_{SR}^{k_1-t+1}e^{\left(-\frac{z}{\bar{\gamma}_E}\right)}}$$
$$\times Y(t+p,1/\bar{\gamma}_E,1). \tag{34}$$

4 Numerical Results

In this section, some typical Monte Carlo (MC) simulations are presented to prove the efficiency of the investigation results. The effects of the key parameters are evaluated. With loss of no generality, in Figs. 2–5, $\bar{\gamma}_{SR}=\bar{\gamma}_{RD}=\bar{\gamma}$, $\delta_R^2=\delta_D^2=\delta_E^2=1$. Besides, $L_{RX_i}=L_{X_iD}=L=20$ and $B=1$. The channel parameters and system parameters are, respectively, given in Tables 2 and 3. Besides, in this paper, the infinite series function is utilized. For example, when $N=2$, 10 terms are acceptable for deriving the proper results. However, when N increases to 5, 20 terms will be required for the simulations. Moreover, in this paper, we used the Matlab for the simulations.

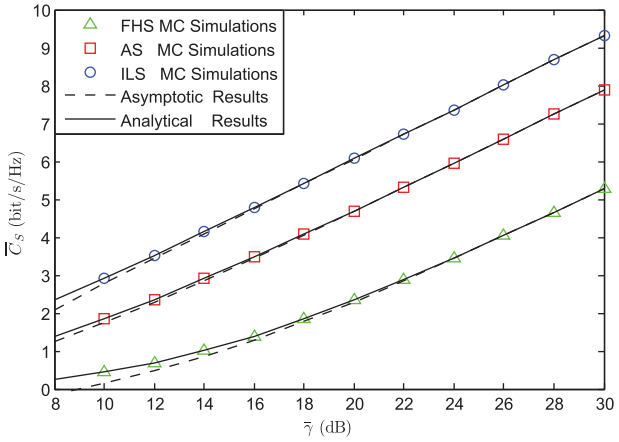

Figure 2: The ASC *vs*. different $\bar{\gamma}$ for three channel fading and $\bar{\gamma}_E=0$ dB with $N=10$

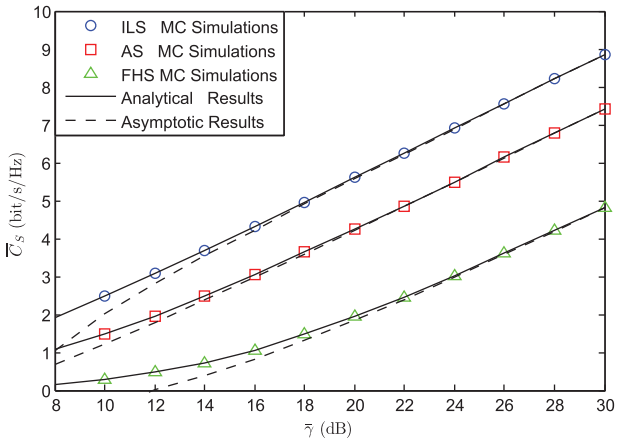

Figure 3: The ASC *vs*. different $\bar{\gamma}$ for three channel fading and $\bar{\gamma}_E = 3$ dB with $N = 10$

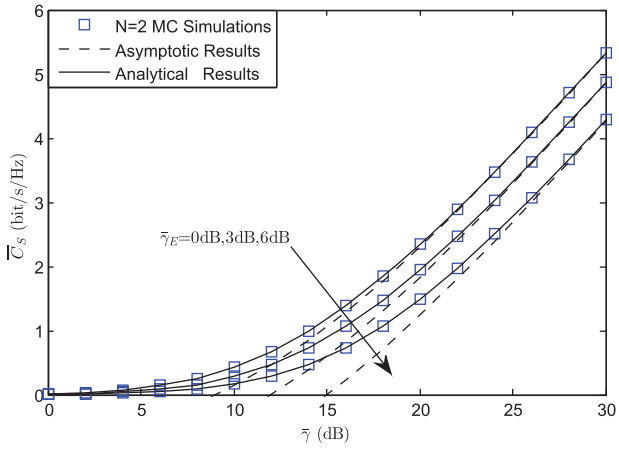

Figure 4: The ASC *vs*. several $\bar{\gamma}$, several $\bar{\gamma}_E$ and $N = 2$ for FHS scenario

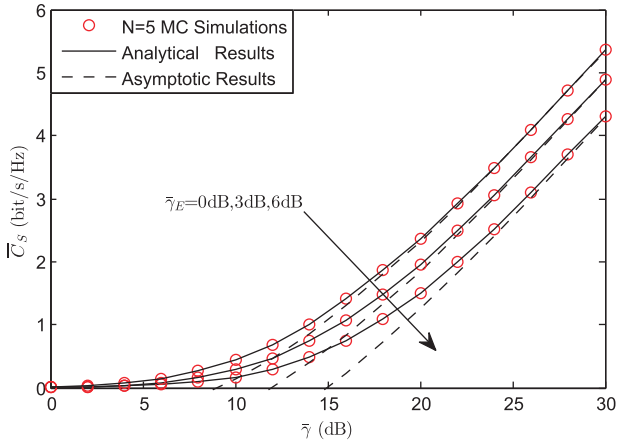

Figure 5: The ASC *vs*. several $\bar{\gamma}$, several $\bar{\gamma}_E$ and $N = 5$ for FHS scenario

Table 2: Channel parameters

Shadowing	m_{SR}	b_{SR}	Ω_{SR}
Average shadowing (AS)	5	0.251	0.279
Infrequent light shadowing (ILS)	10	0.158	1.29
Frequent heavy shadowing (FHS)	1	0.063	0.0007

Table 3: System parameters

Parameters	Value
Satellite orbit	GEO
Frequency band	$f = 2$ GHz
3 dB angle	$\overline{\theta}_k = 0.8^\circ$
Maximal beam gain	$G_{max} = 48$ dB
The antenna gain	$G_{R_e} = 4$ dB

As proved in [34] and [36], a satellite channel model is expected to be general and applicable for a wide range of elevation angles, under which the satellite can be observed. In this regard, the most common approach to evaluate the impact of the elevation angle on channel statistical parameters is based on the transformation from empirical expression. According to [34], the maximum elevation angle is around 80, while the minimum elevation angle is considered to be around 20. In order to tackle the geographical terrain affects. Hence, this is particularly useful when applying a set of data parameters with moderate variation to a model with specific shadowing and infrequent light shadowing conditions (i.e., frequent heavy shadowing, average shadowing and infrequent light shadowing). Please note that for specific shadowing conditions, different parameters have been employed to cover a range of elevation angles in many existing works [17,19].

Fig. 2 plots the ASC *vs.* several $\bar{\gamma}$ for three channel fading and $\bar{\gamma}_E = 0$ dB with $N = 10$. From Fig. 2, it can be got that the simulations are tight across the theoretical analysis, which implies the efficiency of the theoretical ones. Moreover, the approximate analysis matches with the simulations well in high SNR regime. Furthermore, we can find that the channel fading has a great impact on the ASC, i.e., the heavy channel fading brings the a lower ASC. In addition, we find that at high SNRs, the gap between the three curves are fixed, which will guide the engineering design.

Fig. 3 plots the ASC *vs.* several $\bar{\gamma}$ for three channel fading and $\bar{\gamma}_E = 3$ dB with $N = 10$. From Fig. 3, it can be got that the simulations are tight across the theoretical analysis, which implies the efficiency of the theoretical ones. Moreover, the approximate analysis match with the simulations well in high SNR regime. Furthermore, we can find that the channel fading has a great impact on the ASC, namely the light channel fading brings the a larger ASC. When Fig. 2 is compared with Fig. 3, we can also find that when the power of the eavesdropper becomes larger, the ASC will have a lower value.

Fig. 4 illustrates the ASC *vs.* several $\bar{\gamma}$, several $\bar{\gamma}_E$ and $N = 2$ for FHS scenario. From Fig. 4, we also can see that the simulation results are the same with the theoretical results, which imply the correctness of our theoretical analysis. In addition, from this figure, we can find that when $\bar{\gamma}_E$ becomes larger, the ASC will be smaller, for the reason that when the power of the eavesdroppers is smaller, the

eve capacity will be degraded. At the same time, it can be observed that the curves are parallel at high SNRs, which is very interesting.

Fig. 5 examines the ASC *vs.* $\bar{\gamma}$, several $\bar{\gamma}_E$ and $N = 5$ for the FHS scenario. From Fig. 5, we can still find that the MC results are tight across the theoretical results, which also verify the rightness of the theoretical results. Besides, when compared with Fig. 4, it can be obtained that when N becomes larger, the ASC will be enhanced. However, we find that N has little impact on the ASC, for the reason that $R \to D$ link is not the decision link. The satellite transmission link is the decision link. Thus, there is a small gap for ASC between different N. In addition, Fig. 5 shows that the curves are still parallel in a high SNR regime, which is also very interesting.

5 Conclusions

In the section, the summary of this work was given. In this work, we researched the ASC for the RIS-based integrated satellite UAV relay networks. To enlarge the coverage area, the satellite was utilized. In order to enhance the transmission, the UAV was utilized to help the satellite's transmission. Moreover, to save the energy, the RIS was utilized in a high building to enhance the transmission. Thus, the considered secrecy model was proper and acceptable. In particular, the final expressions were obtained for the ASC, and from the derived results, we could get the impacts of key parameters on the ASC. Especially for the asymptotic results, we could observe the following effects: the light channel fading, a lower $\bar{\gamma}_E$ and a larger N would result in a larger ASC. Finally, several simulation results valuated the rightness of both the theoretical and asymptotic analyses.

Acknowledgement: The authors wish to express their appreciation to the reviewers for their helpful suggestions which greatly improved the presentation of this paper. The authors are grateful for the support by National Natural Science Foundation of China.

Funding Statement: This work was supported by the National Natural Science Foundation of China under Grants 62001517 and 61971474, in part supported by the Beijing Nova Program under Grant Z201100006820121.

Author Contributions: The authors confirm contribution to the paper as follows: study conception and design: Ping Li, Kefeng Guo and Feng Zhou; date collection: Ping Li, Kefeng Guo, and Xueling Wang; analysis and interpretation of results: Ping Li, Kefeng Guo, Feng Zhou, Xueling Wang and Yuzhen Huang; draft manuscript preparation: Ping Li, Kefeng Guo, and Feng Zhou. All authors reviewed the results and approved the final version of the manuscript.

Availability of Data and Materials: The raw/processed data required to reproduce the above findings cannot be shared at this time as the data also forms part of an ongoing study.

Conflicts of Interest: The authors declare that they have no conflicts of interest to report regarding the present study.

References

1. Ma, G., Dand, S., Alouini, M. S., Shihada, B. (2022). Smart buildings enabled by 6G communications. *IEEE Internet of Things Magazine, 5(2),* 33–52.

2. Guo, K., Lin, M., Zhang, B., Zhu, W. P., Wang, J. B. et al. (2019). On the performance of LMS communication with hardware impairments and interference. *IEEE Transactions on Communications, 67(2),* 1490–1505.
3. Peng, D., He, D., Li, Y., Wang, Z. (2022). Integrating terrestrial and satellite multibeam systems toward 6G: Techniques and challenges for interference mitigation. *IEEE Wireless Communications, 29(1),* 24–31.
4. Msadaa, I. C., Zairi, S., Dhraief, A. (2022). Non-terrestrial networks in a nutshell. *IEEE Internet of Things Journal, 5(2),* 168–174.
5. Giambene, G., Kota, S., Pillai, P. (2018). Satellite-5G integration: A network perspective. *IEEE Network, 32(5),* 25–31.
6. Lin, M., Huang, Q., Cola, T. D., Wang, J. B., Wang, J. et al. (2020). Integrated 5G-satellite networks: A perspective on physical layer relibility and security. *IEEE Wireless Communications, 27(6),* 152–159.
7. Li, X., Shi, W. (2022). Hybrid satellite-UAV-terrestrial maritime networks: Network selection for users on a vessel optimized with transmit power and UAV position. *China Communications, 19(9),* 37–46.
8. Wu, W., Zhou, F., Wang, B., Wu, Q., Dong, C. et al. (2022). Unmanned aerial vehicle swarm-enabled edge computing: Potentials, promising technologies, and challenges. *IEEE Wireless Communications, 29(4),*78–85.
9. Wu, W., Yang, F., Zhou, F., Wu, Q., Hu, R. Q. (2022). Intelligent resource allocation for IRS-enhanced OFDM communication systems: A hybrid deep reinforcement learning approach. *IEEE Transactions on Wireless Communications, 22(6),* 4028–4042.
10. Guo, K., Lin, M., Zhang, B., Wang, J. B., Wu, Y. et al. (2020). Performance analysis of hybrid satellite-terrestrial cooperative networks with relay selection. *IEEE Transactions on Vehicular Technology, 69(8),* 9053–9067.
11. Guo, K., An, K., Zhang, B., Huang, Y., Guo, D. et al. (2019). On the performance of the uplink satellite multi-terrestrial relay networks with hardware impairments and interference. *IEEE Systems Journal, 13(3),* 2297–2308.
12. Upadhyay, P. K., Sharma, P. K. (2016). Max-max user-relay selection scheme in multiuser and multirelay hybrid satellite-terrestrial relay systems. *IEEE Communications Letters, 20(2),* 268–271.
13. An, K., Lin, M., Ouyang, J., Huang, Y., Zheng, G. (2014). Symbol error analysis of hybrid satellite-terresrial cooperative networks with cochannel interference. *IEEE Communications Letters, 18(11),* 1947–1950.
14. Li, X., Zheng, Y., Khan, W. U., Zeng, M., Li, D. et al. (2021). Physical layer security of cognitive ambient backscatter communications for green Internet-of-Things. *IEEE Transactions on Green Communications and Networking, 5(2),* 1066–1076.
15. Li, B., Fei, Z., Zhou, C., Zhang, Y. (2020). Physical layer security in space information networks: A survey. *IEEE Internet of Things Journal, 69(5),* 33–52.
16. An, K., Lin, M., Ouyang, J., Zhu, W. P. (2016). Secure transmission in cognitive satellite terrestrial networks. *IEEE Journal on Selected Areas in Communications, 34(11),* 3025–3037.
17. Guo, K., An, K., Zhang, B., Huang, Y., Tang, X. et al. (2020). Physical layer security for multiuser satellite communication systems with threshold-based scheduling scheme. *IEEE Transactions on Vehicular Technology, 69(5),* 5129–5141.
18. Guo, K., Li, X., Alazab, M., Jhaveri, R. H., An, K. (2022). Integrated satellite multiple two-way relay networks: Secrecy performance under multiple eves and vehicles with non-ideal hardware. *IEEE Transactions on Intelligent Vehicles, 8(2),* 1307–1318.
19. Guo, K., Dong, C., An, L. (2022). NOMA-based cognitive satellite terrestrial relay network: Secrecy performance under channel estimation errors and hardware impairments. *IEEE Internet of Things Journal, 9(18),* 17334–17347.
20. Guo, K., An, K., Zhang, B., Guo, D. (2018). Physical layer security for hybrid satellite terrestrial relay networks with joint relay selection and user scheduling. *IEEE Access, 6,* 55815–55827.

21. Lin, Z., Lin, M., Champagne, B., Zhu, W. P., Dhahir, N. A. (2021). Secrecy-energy efficient hybrid beamforming for satellite-terrestrial integrated networks. *IEEE Transactions on Communications, 69(3),* 6345–6360.
22. Lin, Z., An, K., Niu, H., Hu, Y., Chatzinotas, S. et al. (2022). SLNR-based secure energy efficient beamforming in multibeam satellite systems. *IEEE Transactions on Aerospace and Electronic Systems, 59(2),* 2085–2088.
23. Chen, Z. N., Qing, X., Tang, X., Liu, W. E. I., Xu, R. et al. (2022). Phased array metantennas for satellite communications. *IEEE Communications Magazine, 60(1),* 46–50.
24. Huang, C., Zappone, A., Alexandropoulos, G. C., Debbah, M., Yuen, C. (2019). Reconfigurable intelligent surfaces for energy efficiency in wireless communication. *IEEE Transactions on Wireless Communications, 18(8),* 4157–4170.
25. Di, B., Zhang, H., Song, L., Li, Y., Han, Z. et al. (2020). Hybrid beamforming for reconfigurable intelligent surface based multi-user communications: Achievable rates with limited discrete phase shifts. *IEEE Journal on Selected Areas in Communications, 38(8),* 1809–1822.
26. Su, Y., Pang, X., Chen, S., Jiang, X., Zhao, N. et al. (2022). Spectrum and energy efficiency optimization in IRS-assisted UAV networks. *IEEE Transactions on Communications, 70(10),* 6489–6502.
27. Yang, L., Meng, F., Zhang, J., Hasna, M. O., Renzo, M. D. (2020). On the performance of RIS-assisted dual-hop UAV communication systems. *IEEE Transactions on Vehicular Technology, 69(9),* 10385–10390.
28. Khalili, A., Malarvizhi, S. (2022). Resource management for transmit power minimization in UAV-assisted RIS HetNets supported by dual connectivity. *IEEE Transactions Wireless Communications, 21(3),* 1806–1822.
29. Nguyen, T. N., Le, H. D., Pham, A. T. (2022). On the design of RIS-UAV relay-assisted hybrid FSO/RF satellite-aerial-ground integrated network. *IEEE Transactions on Aerospace Electronic Systems, Early Access, 3,* 1–15.
30. Guo, K., An, K. (2022). On the performance of RIS-assisted integrated satellite-UAV-terrestrial networks with hardware impairments and interference. *IEEE Wireless Communications Letters, 11(1),* 131–135.
31. Lin, Z., Niu, H., An, K., Wang, Y., Zheng, G. et al. (2022). Refracting RIS-aided hybrid satellite-terrestrial relay networks: Joint beamforming design and optimization. *IEEE Transactions on Aerospace and Electronic Systems, 58(4),* 3717–3724.
32. Guo, K., Liu, R., Dong, C., An, K., Huang, Y. et al. (2023). Ergodic capacity of NOMA-based overlay cognitive integrated satellite-UAV-terrestrial networks. *Chinese Journal of Electronics, 32(2),* 273–282.
33. Zhou, F., Li, X., Alazab, M., Jhaveri, R. H., Guo, K. (2022). Secrecy performance for RIS-based integrated satellite vehicle networks with a UAV relay and MRC eavesdropping. *IEEE Transactions on Intelligent Vehicles, 8(2),* 1676–1685.
34. Abdi, A., Lau, W. C., M., S., Kaveh, M. (2003). A new simple model for land mobile satellite channels: First-and second-order statistics. *IEEE Transactions on Wireless Communications, 2(3),* 519–528.
35. Gradshteyn, I. S., Ryzhik, I. M. (2007). *Table of integrals, series and products*. Boston, USA: Academic Press.
36. Arti, M. K., Suresh, K. J. (2016). OSTBC transmission in shadowed-Rician land mobile satellite links. *IEEE Transactions on Vehicular Technology, 65(7),* 5771–5777.